NBSIR 83-2755

Development of Power System Measurements -- Quarterly Report October 1, 1982 to December 31, 1982

U.S. DEPARTMENT OF COMMERCE
National Bureau of Standards
Center for Electronics and Electrical Engineering
Electrosystems Division
Washington, DC 20234

September 1983

Prepared for
Department of Energy
Division of Electric Energy Systems
[illegible]0 Independence Avenue, SW
[illegible]shington, DC 20585

NBSIR 83-2755

DEVELOPMENT OF POWER SYSTEM MEASUREMENTS -- QUARTERLY REPORT OCTOBER 1, 1982 TO DECEMBER 31, 1982

R. E. Hebner, Editor

U.S. DEPARTMENT OF COMMERCE
National Bureau of Standards
Center for Electronics and Electrical Engineering
Electrosystems Division
Washington, DC 20234

September 1983

Prepared for
Department of Energy
Division of Electric Energy Systems
1000 Independence Avenue, SW
Washington, DC 20585

U.S. DEPARTMENT OF COMMERCE, Malcolm Baldrige, *Secretary*
NATIONAL BUREAU OF STANDARDS, Ernest Ambler, *Director*

Foreword

This report summarizes the progress on five technical investigations during the first quarter of FY 1983. Although reasonable efforts have been made to ensure the reliability of the data presented, it must be emphasized that this is an interim report so that further experimentation and analysis may be performed before the conclusions from any of these investigations are formally published. It is therefore possible that some of the observations presented in this report will be modified, expanded, or clarified by our subsequent research.

TABLE OF CONTENTS

LIST OF FIGURES

LIST OF FIGURES

LIST OF TABLES

DEVELOPMENT OF POWER SYSTEM MEASUREMENTS -- QUARTERLY REPORT

October 1, 1982 to December 31, 1982

R. E. Hebner, Editor

This report documents the progress on five technical investigations sponsored by the Department of Energy and performed by the Electrosystems Division, the National Bureau of Standards. The work described covers the period from October 1, 1982 to December 31, 1982. The report emphasizes the calibration of instruments designed to measure the 60-Hz electric and magnetic fields in biological exposure facilities, the measurement of the rate of decomposition of SF_6 in positive dc-corona discharges, and in the measurement of space charge in transformer oil between 100°C and 150°C.

Key words: cables; composite insulation; dc fields; high voltage; incipient fault; insulation; liquid breakdown; SF_6; space charge; transformer oil.

1. INTRODUCTION

Under an interagency agreement between the U. S. Department of Energy and the National Bureau of Standards, the Electrosystems Division, NBS, has been providing technical support for DOE's research on electric energy systems. This support has been concentrated in the following areas -- the measurement of electric and magnetic fields, the measurement of partial discharge phenomena, and the measurement of interfacial electrostatic field distributions and of space charge density. The technical progress made during the quarter October 1, 1982 to December 31, 1982 is summarized in this report.

2. DC FIELDS AND ION MEASUREMENTS
Subtask No. A018

The objectives of this investigation are to develop methods to evaluate and calibrate instruments which are used, or are being developed, to measure the electric field, conductivity, the space charge density, and current density in the vicinity of high-voltage dc transmission lines and in apparatus designed to simulate the transmission line environment; to provide electrical measurement support of DOE-funded efforts to determine the effects of ac fields on biological systems and to provide similar support for biological studies which will be funded by the State of New York.

During the current reporting period, an apparatus for simultaneously generating a 60-Hz rotating magnetic field and a 60-Hz vertical electric field was assembled. The apparatus consists of two Helmholtz coils oriented orthogonally relative to one another and placed in the NBS parallel plate system. A schematic view of the system is shown in figure 1. One of the magnetic field components is aligned with the vertical electric field. As a result, the rotating magnetic field is in a vertical plane. This apparatus was developed in support of the New York State-funded biological studies in which animals will be simultaneously

exposed to a rotating magnetic field and vertical electric field. Several in vitro and one human study are also planned. A requirement for the animal and human studies is that the electric field and magnetic field both be aligned vertically when the electric field reaches its maximum value. When this condition is satisfied, it can be shown that the Lorentz force on charges moving within the body can, under certain conditions, reach its maximum magnitude.

The NBS apparatus was used to determine how accurately one can measure, using a dual beam oscilloscope, the phase relations between the two opthogonal magnetic field components, which must be in quadrature, and between the vertical magnetic field and the electric field, which must be in phase. If it can be shown that the phase relations between the various field components can be determined to within a few degrees, researchers can establish the proper phase relations without the use of costly phase measuring instrumentation. Included in the NBS apparatus was a phase shifter, which could vary the phase difference between the sinusoidal signals that were amplified and used to energize the Helmholtz coils and parallel plates. Also part of the apparatus was a phase meter which could measure the phase difference between two signals from sensors in the field.

When determining phase relations between the different field components, the phase shifts introduced by the field-sensing transducers should be noted. The sensors used to observe the magnetic field waveforms were two "pick-up coils" which are electrically shielded loops of many turns. The sensor for observing the electric field waveform (not shown in fig. 1) was a flat plate. Currents induced in the plate by the electric field were measured with a current-to-voltage operational amplifier circuit. The voltages from the magnetic field sensors will be shifted in phase by -90° because of Faraday's Law. That is, the electromotive force (EMF) from the sensing coil is given by

$$EMF = -N(d\phi/dt) = -(N\omega B \cos \omega t) \times (\text{coil area}),$$

where the flux ϕ is given by

$$\phi = (B \sin \omega t) \times (\text{coil area}),$$

and N and B are the number of turns of wire in the sensor and B is peak value of the flux density. No further significant phase changes occur in the circuit with the oscilloscope and the phase meter because the output impedance of the sensor coil is very small compared to the input impedances of the oscilloscope and phase meter.

Similarly, the induced current from the plate sensor is 90° phase with respect to the electric field. This current is typically detected with electronic circuitry which can also affect the phase relationships. For example, a current-to-voltage inverting operational amplifier circuit with resistive feedback will shift the phase of the current waveform by 180°. The output voltage from the amplifier will thus be -90° out of phase with the electric field.

Because the parallel plates are also in the magnetic field, eddy currents are produced in the plates and the magnetic field from the eddy currents will perturb the field that produces it. Because of Lenz's Law, the field from the eddy currents will retard the Helmholtz coil field and decrease the maximum value (i.e., superposition of fields.) However, this perturbation of the

magnetic field will decrease as some function of distance away from the parallel plates or eddy currents. The implication of this effect for the New York State biological studies is that when measurements of the circularly polarized magnetic field are made, the measurements should be performed at the location where the test animals will be placed (usually the bottom plate of the parallel plate system) and not, for example, midway between the plates. Similarly, when the phase relation between the vertical magnetic field and electric field are examined, it should be done near the animal location.

All of the above remarks regarding the phases of the field probe signals and perturbation of the ambient field by eddy currents have been confirmed experimentally with the apparatus shown in figure 1.

To determine experimentally how accurately an oscilloscope can measure phase differences between two sinusoidal signals, the case of two sine waves 90° out of phase was examined. Figure 2(a) shows half a cycle of two sinusoidal signals centered on an oscilloscope screen. The phase difference between the two signals was simultaneously measured with the phase meter and equaled 90°, confirming the visual observation. Greater precision can be obtained with the oscilloscope measurement, however, by expanding the vertical scale of one of the waveforms as shown in figure 2(b). The zero crossings of the expanded waveform are symmetrically located with respect to the zero crossing of the unexpanded signal. Figure 2(c) shows the effect on the oscilloscope display of changing the phase between the signals by 4.5°. This difference can be calculated with fair accuracy by noting the shift of ~ 0.025 percent (1/40) of the expanded waveform along the horizontal axis. This measurement technique assumes that overdriving the oscilloscope amplifier does not introduce asymmetry in the amplified waveform.

The electric field mill which was tested during the previous reporting period was returned to the manufacturer for several modifications. Measurements at NBS had revealed that surface charging of some exposed circuit board near the stator of the field mill resulted in field strength values that were too low. Upon being informed of our test results, the manufacturer has redesigned the field mill sensing head, eliminating the exposed dielectric surface. This change as well as several other adjustments were performed on our unit under warranty. The field mill has been returned to NBS and recent measurements indicate that the device is functioning properly in the presence of space charge.

NBS hosted a two-day Workshop on Measurement of the Electrical Environment Near High-Voltage DC Transmission Lines in October. The meeting brought together individuals interested in the state-of-the-art electric field and ion-related measurements near HVDC transmission lines and in biological exposure systems. Measurement problems which require further study were identified and include: measurements of ion density above and at ground level, measurement of ion mobility spectra, and identification of ion species. An increased interest in measurements off the right-of-way was also shown.

The first revision of an existing IEC draft standard on power frequency electric field measurements was completed at NBS and distributed to members of a newly formed IEC working group for comments. This latest version of the draft includes changes that were agreed to by the parent IEC technical committee (TC42) as well as some observer proximity effect data measured several years ago by NBS staff.

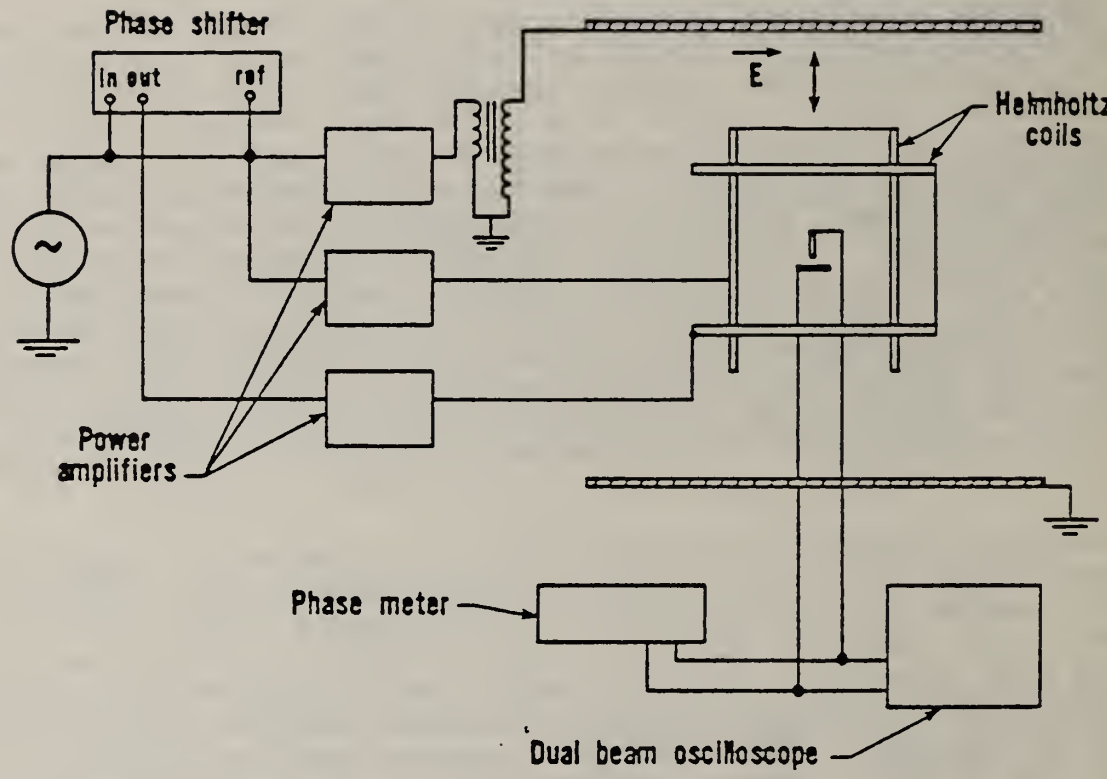

Figure 1. Schematic view of apparatus used to generate 60 Hz electric and magnetic fields. Circularly polarized magnetic fields can be obtained with the orthogonally oriented Helmholtz coils.

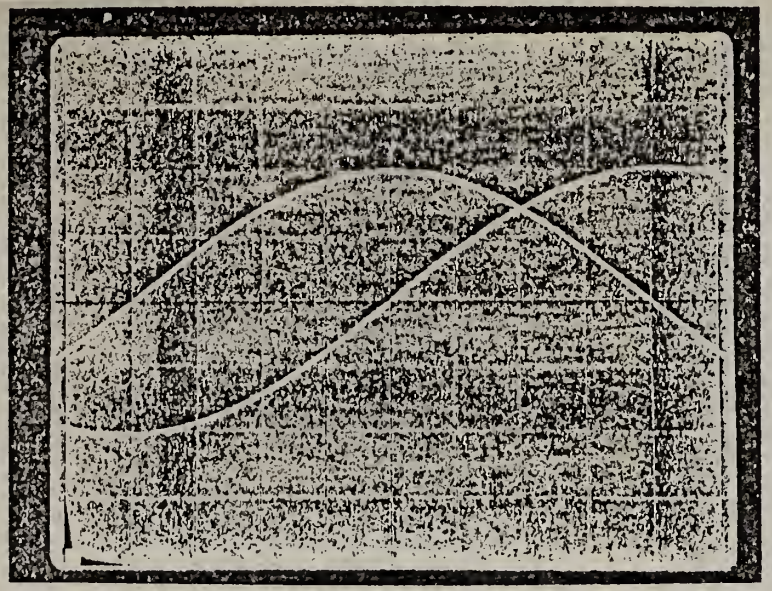

Figure 2(a) Waveforms 90 degrees out of phase.

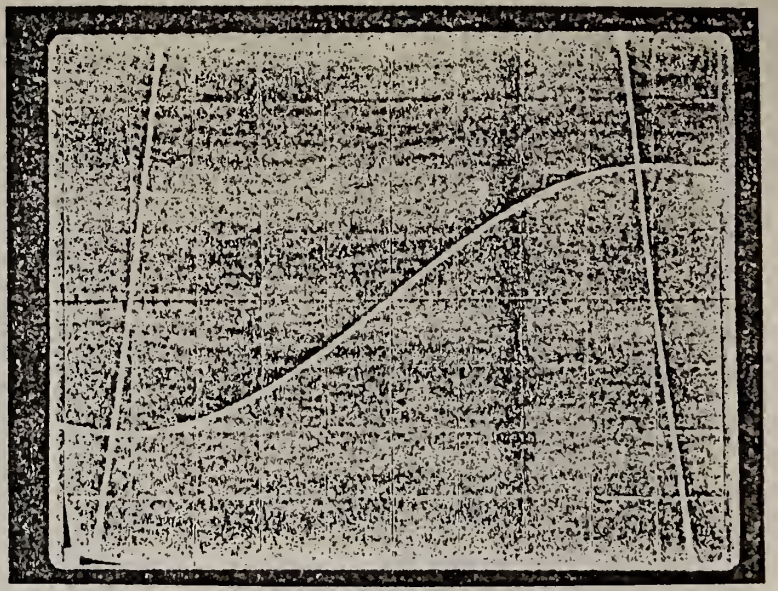

Figure 2(b) Waveforms 90 degrees out of phase.

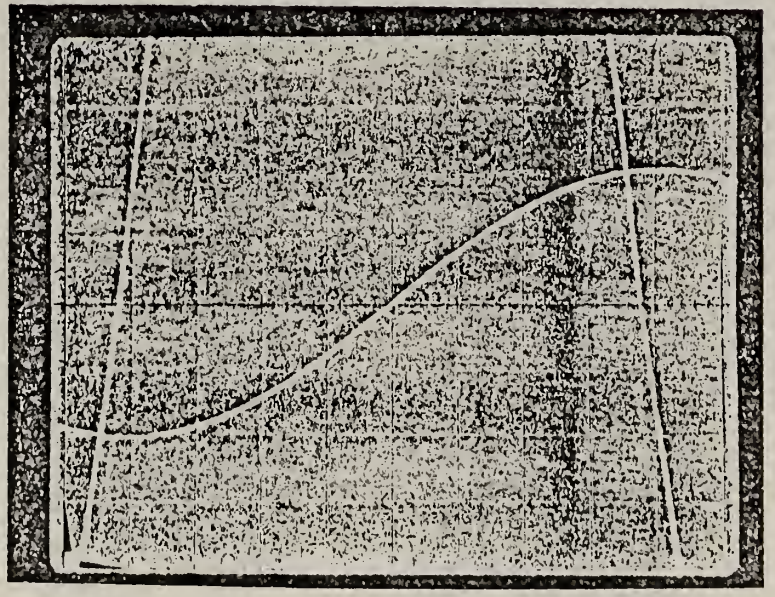

Figure 2(c) Displacement produced by 4.5 degree shift in phase is readily observed.

During the next quarter, problems associated with ion density measurements above and at ground level will continue to be studied. Additional measurements are planned with an ion counter operating above the ground plane. The first measurements with an ion counter operating in the ground plane are also planned. Preliminary theoretical calculations suggest some possible measurement problems when the ion counter is used in the ground plane of a parallel plate or coaxial cylinder apparatus. Several visits to laboratories funded by New York State are expected during the next quarter (none occurred during the last quarter) and some on-site field measurements will likely be made. Comments from the newly formed IEC working group members who are preparing a draft standard for power frequency electric field measurements will be sent to NBS during the next quarter and the second revision of the draft will be written at NBS.

For further information, contact Dr. M. Misakian (301) 921-3121.

3. TECHNICAL ASSISTANCE FOR FUTURE INSULATION SYSTEMS RESEARCH
Subtask No. A053

The objective of this project is to develop diagnostic techniques to monitor, identify, and predict degradation in future compressed gas electrical insulating systems under normal operating conditions. The focus is on the fundamental information and data needed to improve test design and performance evaluation criteria. The investigation of partial discharges (corona) in gaseous dielectrics is emphasized. This phenomenon gives rise to degradation of the gas under high electrical stress which leads to breakdown. Measurement of partial discharge inception in highly nonuniform fields may prove to be a preferred method to determine dielectric strength of electronegative gases.

The planned activities for FY83 include:

1) Preparation of conference and archival papers on the effect of radiation in enhancing electric discharge initiation near a positively stressed electrode in compressed SF_6 and O_2;

2) Extension of our previous measurements [1] of the production rates of oxyfluorides in SF_6 corona discharges to include negative discharges as well as other gas pressures and discharge power levels, and preparation of the results for publication in an archival paper;

3) Identification of the predominant gaseous decomposition products from corona in one or more of the following gas mixtures: $SF_6 + N_2$, $SF_6 + CO_2$, and $SF_6 + c\text{-}C_4F_8 + CHF_3$;

4) Evaluation of a thin-film, aluminum oxide hygrometer probe for calibration of a gas chromatograph-mass spectrometer (GC/MS) used to measure trace quantities of water vapor in SF_6 and other gaseous dielectrics, and extension of our previous measurements on the effects of trace levels of H_2O on electron avalanche growth and corona discharge characteristics in SF_6; and

5) Design and construction of a drift tube-mass spectrometer system to evaluate measurements proposed to identify and characterize corona-generated ion species in air, SF_6, and other gas dielectrics.

Activity 1) was completed during this past quarter. A paper describing the results of our measurements and theoretical analysis was presented at the 35th Annual Gaseous Electronics Conference and a manuscript was prepared for submission to the Journal of Applied Physics. Considerable time was also devoted to activity 2). The results of this work are highlighted in this report. Concerning activity 4), a thin-film aluminum oxide hygrometer system for measurement of water vapor content in gaseous dielectrics was received and subjected to preliminary tests.

The computer software, which was developed to extract molecular species production rates from GS/MS data, underwent a thorough evaluation under a wide range of data conditions. Some improvements were made which allow a more rapid and reliable analysis of data. The results reported were obtained with the use of this software.

Our earlier measurements [1] of the production rates of SOF_2 and SO_2F_2 from positive corona discharges in SF_6 have been extended to other pressures and discharge power levels. Because of improvements in the analytical techniques used and inclusion of correction factors for discharge power variations, the data presented here are considered to be more reliable than those previously reported [1]. However, it should be cautioned that a thorough error analysis has not yet been applied and, therefore, even these data must be considered preliminary in the sense that no estimated uncertainties are given. We feel, nevertheless, that the data are sufficiently reliable to reveal certain trends.

Examples of production rate results obtained from recent analysis of data are given in Tables 1-3. Tables 1 and 2 apply, respectively, to the oxyfluorides SOF_2 (thionylfluoride) and SO_2F_2 (sulfurylfluoride). Given in these tables are the production rates of those species in nanomoles per joule at the different indicated gas pressures and discharge power levels, and for accumulated energies, U, dissipated in the discharge of 10 kJ and 15 kJ. These tables also give the maximum observed production rates at the highest accumulated energy dissipated and the exponential fitting parameter ε with which the production can be described using the assumed form

$$C = AU^{1+\varepsilon}, \qquad (1)$$

which appears to be adequate to describe the production over the range of energies used in the measurements. Here C is the concentration in moles and A is a constant. The parameters ε and A are determined from a least squares fit of the form (1) to each set of experimental data $\{C_m(t), U(t)\}$, as illustrated in figure 3. Here $C_m(t)$ and $U(t)$ are, respectively, the measured concentrations and accumulated energies at times t.

For our experimental conditions where the gas volume is 4.0 liters and the temperature is 300°K, the measured concentrations C_m in moles are given by

$$C_m = 1.625 \times 10^{-9}\ P\ C_r(q_m/q_r), \qquad (2)$$

Table 1. Measured production rates for SOF_2 in SF_6 at the different indicated gas pressures and discharge power.

Gas pressure (kPa)	Ave. discharge power (mW)	Ion monitored (m/e)	Measured production rates (n moles/J)* (U = 10 kJ)	(U = 15 kJ)	(max.)	ε
116	804	86	0.4	0.5	1.3	0.590
200	335	67	4.2	4.9	5.0	0.347
200	335	86	4.3	5.0	5.1	0.335
200	777	67	2.6	3.3	4.1	0.582
200	777	86	2.5	3.4	4.7	0.785
300	198	86	3.3	4.9	6.0	1.018
300	430	86	2.0	2.6	3.9	0.653
300	945	86	1.0	1.4	3.8	0.817

*1 n mole = 10^{-9} moles

Table 2. Measured production rates for SO_2F_2 in SF_6 at the different indicated gas pressures and discharge power.

Gas pressure (kPa)	Ave. discharge power (mW)	Ion monitored (m/e)	Measured production rates (n moles/J)*			ε
			(U = 10 kJ)	(U = 15 kJ)	(max.)	
116	804	83	0.6	0.7	2.0	0.667
200	335	83	3.2	3.7	3.7	0.326
200	335	102	3.4	4.1	4.2	0.335
200	777	83	1.7	2.0	2.5	0.460
200	777	102	1.7	2.0	2.5	0.485
300	198	83	1.8	2.3	2.6	0.658
300	430	83	1.6	1.9	2.4	0.362
300	945	83	0.7	0.9	2.1	0.664

*1 n mole = 10^{-9} moles

Table 3. Ratios of production rates for SOF_2 and SO_2F_2 at the indicated gas pressures and discharge power.

Gas pressure (kPa)	Discharge power (mW)	$r(SOF_2)/r(SO_2F_2)$ (U = 15 kJ)
116	804	0.73
200	335	1.36
	777	1.67
300	198	2.13
	430	1.39
	945	1.45

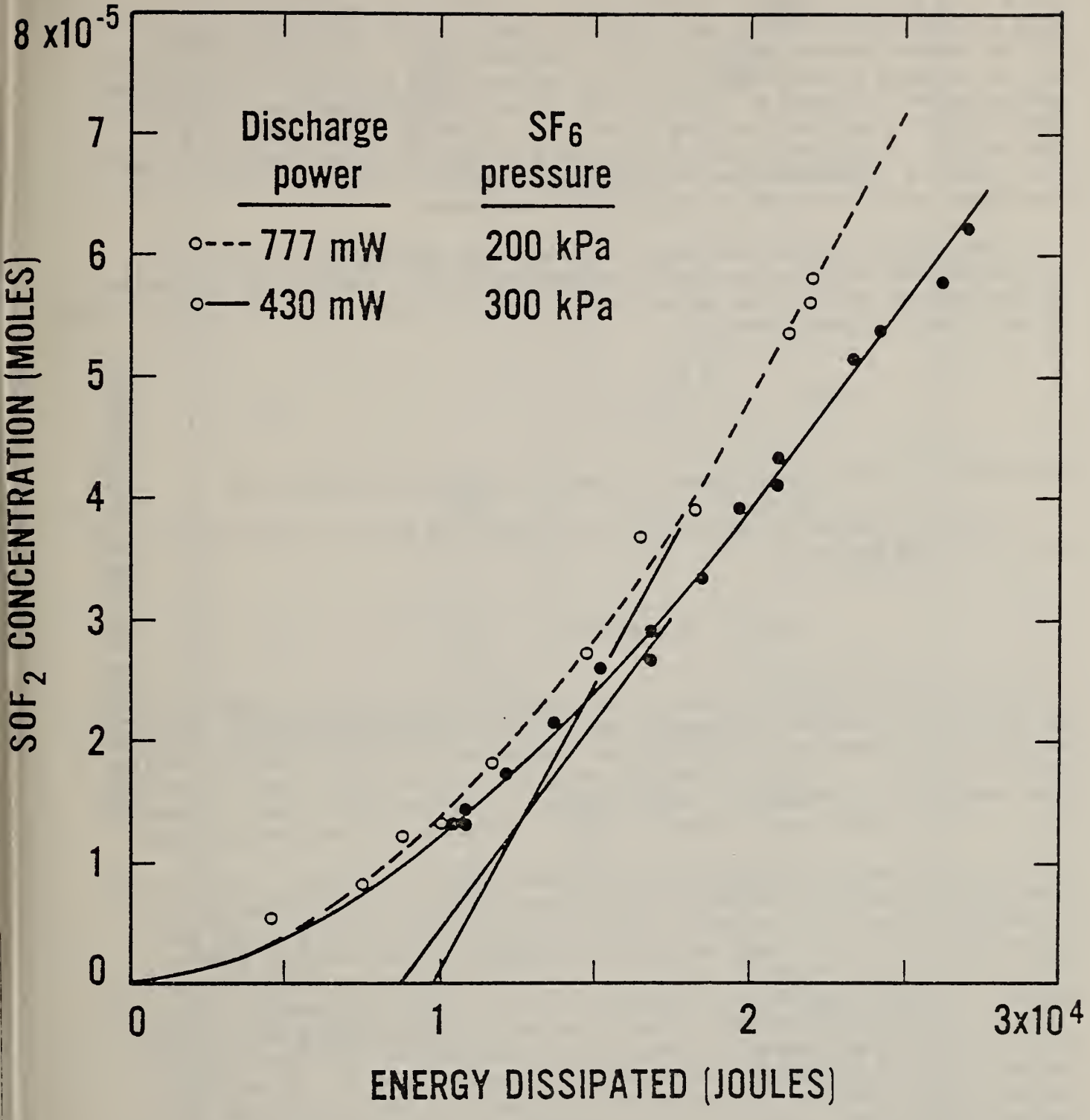

Figure 3. Measured concentration of SOF_2 in moles as a function of accumulated energy dissipated by a positive-dc corona discharge in SF_6 for the indicated discharge power levels and gas pressures.

where P is the gas pressure in kPa, C_r is the reference concentration in moles from a standard gas sample, and (q_m/q_r) is the ratio of the GC/MS response for the unknown sample to that of the reference sample. The values of q_m and q_r are obtained from a computer analysis of the GC/MS single-ion chromatograms such as shown in figure 4. The analysis takes into consideration interference from adjacent peaks and can give q_m and q_r in terms of either peak area or peak height. In general, peak height and area results agree favorably; however, the latter is considered more reliable under conditions where variations in peak shape are significant during a given experiment.

The results reported here were obtained from measurements in which the average corona discharge current I was held constant. Treating the discharge as a dc-current source, the accumulated energy dissipated, U(t), in the discharge at any time t is then given by

$$U(t) = I \int_0^t V(t')dt', \qquad (3)$$

where V(t') is the instantaneous voltage drop across the corona cell.

The rates quoted in the tables are derived from the fits according to eq (1) using the relationship

$$r = dC/dU = (1 + \varepsilon)AU^{\varepsilon}. \qquad (4)$$

It should be cautioned that there is no fundamental basis for believing that eqs (1) and (4) provide an adequate description for arbitrarily large dissipation energies and, therefore, extrapolations much above the maxima reported here may not be valid. In fact, it appears from the data analyzed thus far that at high enough U, the production rates approach a constant value (see, for example, fig. 1), and at that point a simple linear fit to the data may be justified.

From the results presented here, certain trends are evident. First, there appear to be no dramatic changes in the production rates with either pressure or discharge power. All of the results for both SOF_2 and SO_2F_2 appear to lie roughly within the range of 0.5 to 6.0 n moles/J, which agrees favorably with our previously reported estimates as well as with those of Castonguay [1]. However, for both species, there appears to be a gradual decrease in production rates with increasing discharge power. Between 200 and 300 kPa there appears to be no significant change in the pattern of decomposition as manifested in ratios of the SOF_2 to SO_2F_2 concentrations given in Table 3. Below 200 kPa the data show a reversal in the relative production rates of SOF_2 and SO_2F_2. Further evidence of a change at lower pressures is provided by a comparison of the chromatograms for the different indicated pressures given in figure 4, which shows a noticeable change in the relative production of SOF_4 compared to SOF_2.

Further measurements are needed to substantiate these trends and thus it would be premature at this stage to attempt an explanation. It is perhaps worth noting, however, that formation of both SOF_4 and SO_2F_2 is believed to depend on the presence of free oxygen in the discharge [1]. Also, SOF_4 can convert to SO_2F_2 through the reaction

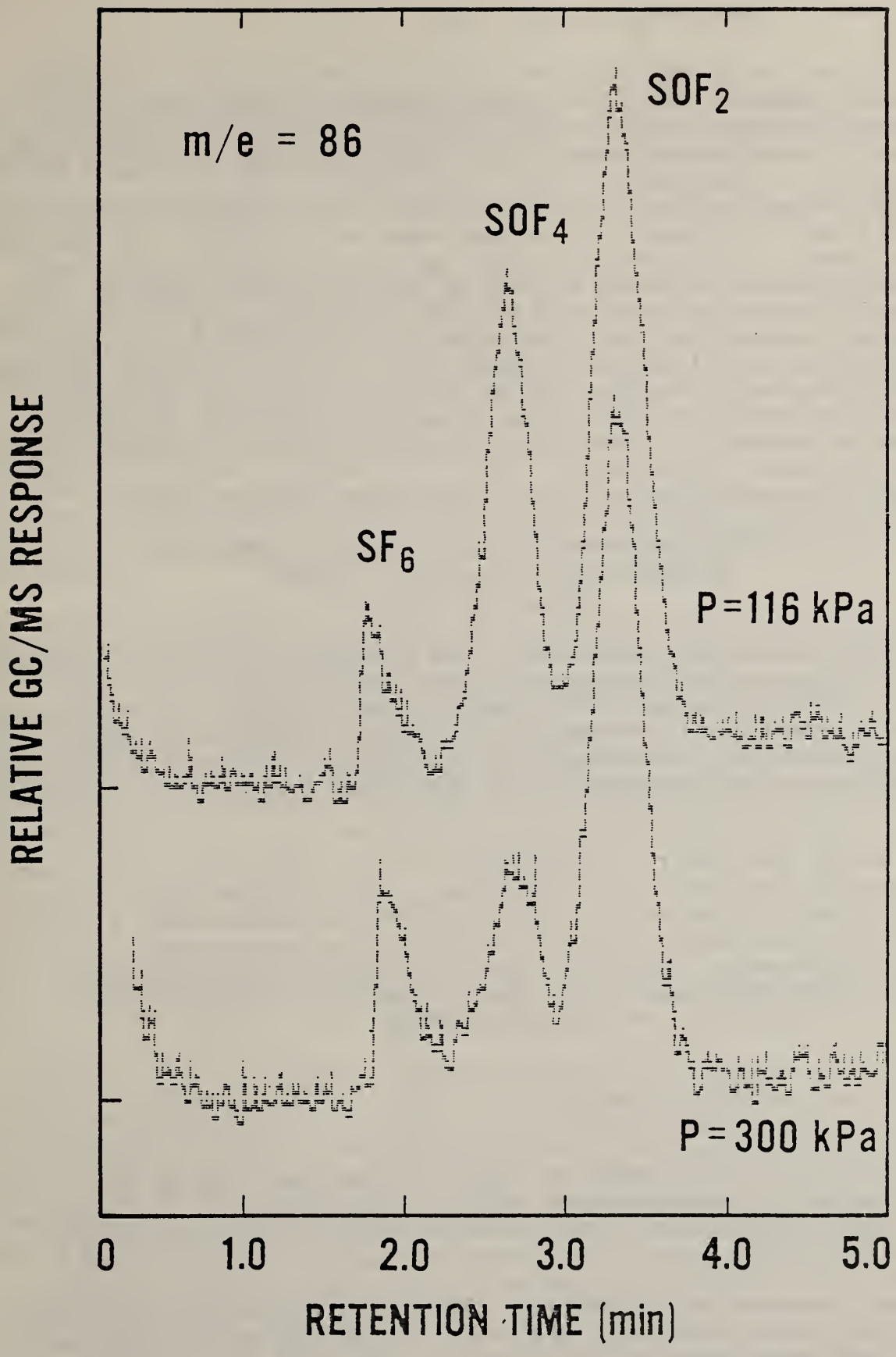

Figure 4. Single-ion chromatograms for ions with mass-to-charge ratio (m/e) of 86 (in a.u.) corresponding to SF_6 degraded by corona discharges for the indicated gas pressures.

$$SOF_4 + H_2O \rightarrow SO_2F_2 + 2HF.$$

One, therefore, expects that any discharge parameter which can affect the relative availability of oxygen or water vapor in the discharge region will also affect the relative production of the various observed oxyfluoride species.

During the next quarter, we plan to continue the measurements of oxyfluoride production rates from corona in SF_6 as described in this report. The measurements will be extended to include not only other gas pressures and discharge power levels, but also negative corona to check on possible polarity effects. More attention will also be given to error analysis and determination of the uncertainties in the measured production rates. The objective is to bring this series of measurements to a conclusion so that preparation of an archival paper describing these results can begin. Further testing of the thin-film aluminum oxide hygrometer probe method for calibration of the GC/MS system for quantitative water vapor measurements in SF_6 should also be carried out in the next quarter.

For further information, contact Dr. R. J. Van Brunt (301) 921-3121.

4. OPTICAL MEASUREMENTS FOR INTERFACIAL CONDUCTION AND BREAKDOWN IN INSULATING SYSTEMS
Subtask No. A057

The objectives of this investigation are to develop apparatus and appropriate procedures for the optical measurements of interfacial electric field and space-charge density in materials for electric power equipment and systems, to understand the interfacial prebreakdown and breakdown processes in specific insulating systems, and to demonstrate the applicability of the developed instrumentation and the procedures in the development and design of future systems.

Last quarter the electric field between parallel plates with a pressboard spacer separating the plates was investigated. Since the electrical strength of that interfacial system was much lower than without an interface, electrical breakdown would occur before reasonable electro-optical measurements could be performed. For example, if the cell constant V_m were 170 kV and typical breakdown voltages were around 30 kV, then the maximum transmittance I/I_m through the cell due to the Kerr effect, given by

$$I/I_m = \sin^2[(\pi/2)(V/V_m)^2], \qquad (5)$$

is $I/I_m = 2.4 \times 10^{-3}$. This amount of light is of the same order as the transmittance due to imperfections in the optics used to monitor the Kerr effect or depolarization of the light from particles or thermal turbulence. Usually the transmittance must be more than 10^{-2} before field measurements can be made. The difficulty was handled by doping the transformer oil with nitrobenzene to enhance the Kerr effect. The results showed that there were no differences in the space-charge distribution along the interface than away from the interface with the application of dc. Thus, the electric field was not changed (at least macroscopically) by the interface.

During this reporting period a method was developed to perform field measurements in non-doped transformer oil at relatively low voltages -- much lower than the typical breakdown voltages for interfacial systems. A comparison of the field near the interface with the field away from the interface was then made under a variety of conditions of water contamination and temperature. In all cases the electric field between the plates was not affected by the presence of the interface.

The increase in sensitivity was obtained by adding an impulse to the steady-state voltage. It is known that the impulse strength of a liquid is greater (often by a factor of two or more) than the dc or 60-Hz ac strength. Because larger impulse voltages can be applied to the cell, the electro-optical transmittance will be larger and, thus, easier to measure, see eq (5). The impulse generator is capacitively coupled to the cell so that an impulse can be applied on top of the steady-state voltages (see fig. 5). This technique exploits the fact that in insulating liquids the macroscopic space-charge development occurs on a millisecond time scale [3,4]. Thus the space charge distribution will result from the steady-state voltage and the microsecond duration pulse will have no affect on the space charge except to enhance its detectability.

To see the advantage of using an impulse voltage in this way, consider an example of our cell. At room temperature, the cell constant is 170 kV. Without an impulse, a 10 kV dc voltage would produce a transmittance, according to eq (1), of $I_{10}/I_m = 3.0 \times 10^{-5}$ which cannot normally be detected since both turbulence and imperfections in the optics dominate such a signal. With a 90 kV impulse the transmittance becomes $I_{90}/I_m = 0.18$. If the 90 kV impulse is added to a 10 kV dc voltage, the 100 kV result produces a transmittance of $I_{100}/I_m = 0.27$. The benefit is shown by the increase of the 10 kV dc signal with the impulse over the 10 kV dc signal without the impulse

$$(I_{100} - I_{90})/I_{10} = 3000,$$

that is, the 90 kV impulse has rendered a 10 kV dc signal 3000 times more observable. (See figure 6 for an example of data.)

With this sensitive system, no space charge was observed at room temperature or at 120°C. Even upon the addition of an estimated 40 ppm of water, no space charge was evident which would produce more than a 10% modification of the field throughout the gap. It must be kept in mind that because of the presence of an interface [made of polytetrafluoroethylene (PTFE)], the cell could not withstand 30 kV dc for long periods of time. Hence it was not possible to explore the field intensities which were previously used to observe space charge in pure transformer oil.

A reasonable hypothesis is suggested from previous observations of space charge in nitrobenzene: space charge may have an onset field which, in this case, is larger than the breakdown field with an interface present. This would explain why space charge could not be observed at the relatively low fields used with the interface but were observed earlier in transformer oil (without an interface) at higher field strengths. This hypothesis will be explored next quarter where no interface will be present and various levels of

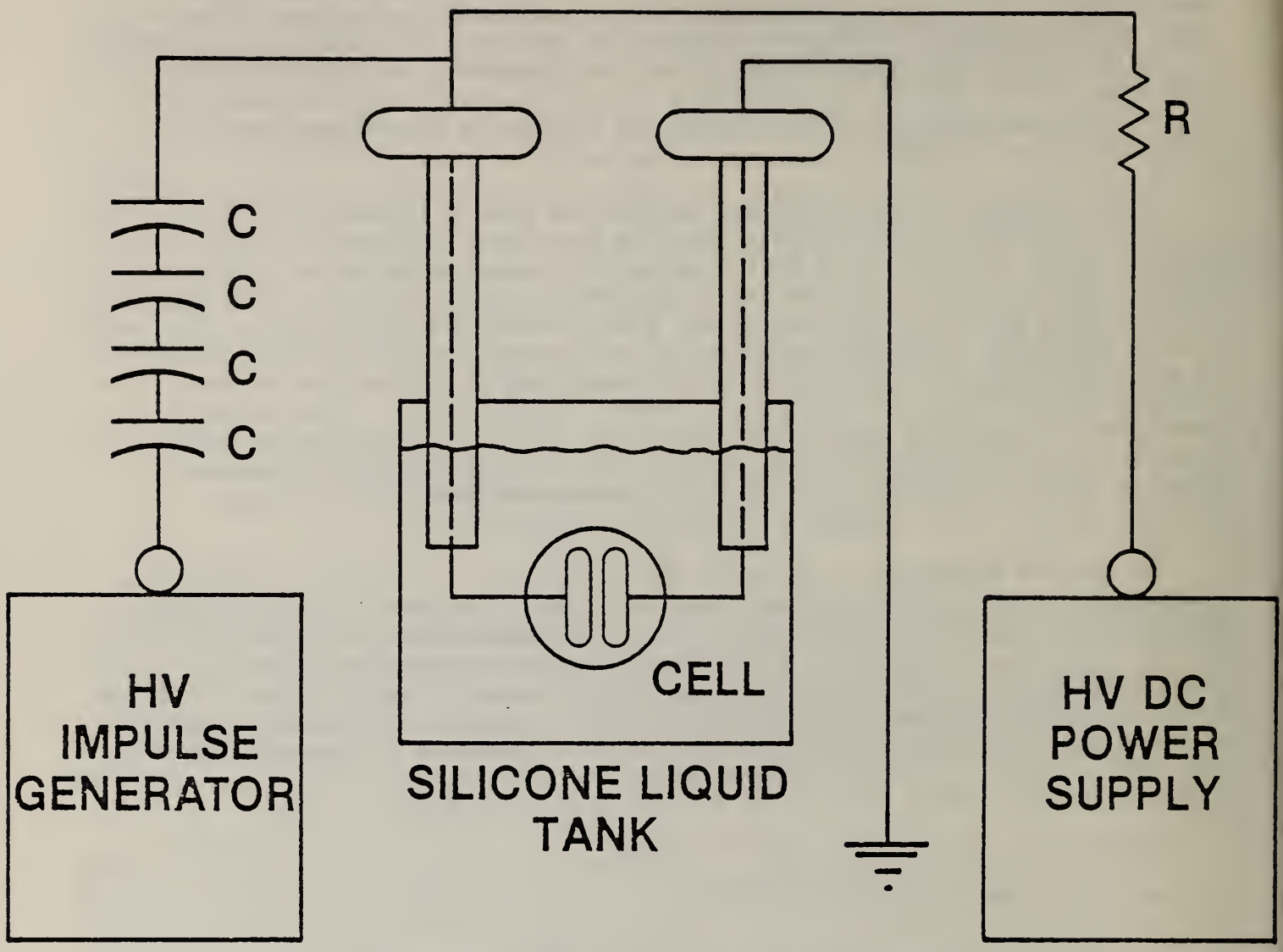

Figure 5. Circuit diagram showing the application of an impulse generator to enhance the transmittance ratio of the coil. Isolation from the dc supply is accomplished via four capacitors in series with a total capacitance of about 1 nF. The current limiting dc resistor is 800 kΩ. Voltage is applied to the closed cell via feed-throughs in the tank's top. The cell has its own oil circulation system (not shown) outside the tank.

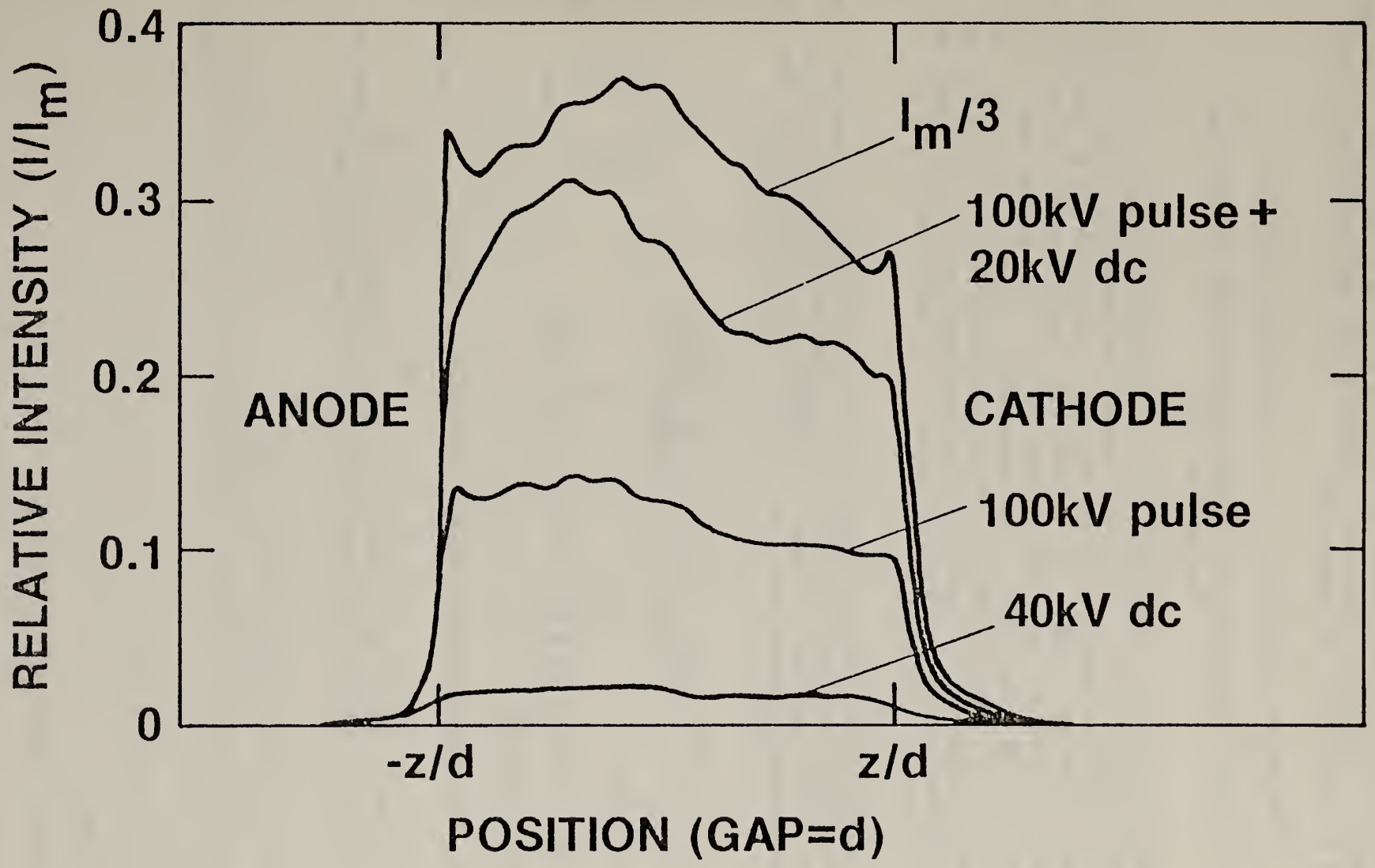

Figure 6. Data showing the usefulness of the impulse-enhancement of lower dc voltages in making the Kerr effect more observable. One third the maximum signal is shown compared to dc alone, pulse alone, and pulse plus dc.

contaminants will be investigated. Additionally, a careful determination of the Kerr coefficient of transformer oil will be made as a function of temperature and wavelength. Finally, a pressboard interface will be installed and its effect upon the field will be determined.

For further information, contact Dr. E. F. Kelley (301) 921-3121.

5. ACTIVE INSULATORS FOR INSULATION AND SURGE SUPPRESSION
Subtask No. AU57

The objective of this investigation is to evaluate the practicality of using active insulators, i.e., insulators made from materials whose resistance is a function of the voltage across the device, to minimize the effects of switching and lightning surges. The theoretical aspect consists of the development of a mathematical model of an electric power system which can be used to predict the effects of active insulators. (The experimental aspect consists of the development of a facility to fabricate insulation materials suitable for use in an active insulator.) This work is being performed by the Department of Electrical Engineering, University of Southern California, under a grant from the National Bureau of Standards.

The single-phase mathematical models for the lightning transient performance of active insulators has been completed. The equivalent model circuit for lightning striking on a tower is shown in figure 7, and the resultant nonlinear equation after substitution is

$$[K\, U_A(t)]^{\alpha} + \frac{A}{1+A \cdot R_t}\, U_A(t) + \frac{B}{1+A \cdot R_t} = 0 , \qquad (6)$$

where $A = 1/Z + 1/Z$

$$B = I_{n,n-1}(T-\tau/m) + I_{n,n+1}(t-\tau/m) + 2\, Is(t)\, Rt/z ,$$

and the nodal voltage is

$$U_n(t) = U_A(t) + \{[K\, U_A(t)]^{\alpha} + Is(t)\} \cdot Rt \ldots \qquad (7)$$

The equivalent circuit for lightning striking directly on the conductor is shown in figure 8, and the nonlinear equation after substitution is

$$[K\, U_A(t)]^{\alpha} + \frac{A}{1+A \cdot R_t}\, U_A(t) + \frac{B}{1+A \cdot R_t} = 0 , \qquad (8)$$

where $A = 1/Z + 1/Z + 1/Z$

$$B = I_{n,n-1}(t-\tau/m) - I_s(t) .$$

The nodal voltage is

$$U_n(t) = U_A(t) + [K\, U_A(t)]^{\alpha} \cdot R_t .$$

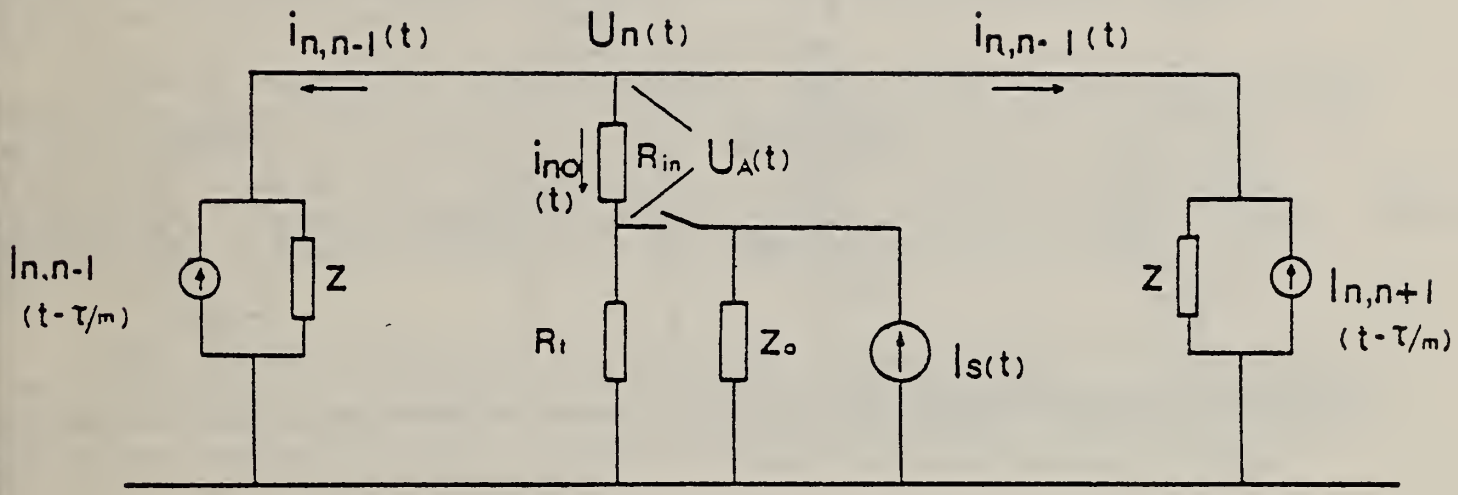

Figure 7. Equivalent circuit model for lightning striking on transmission tower.

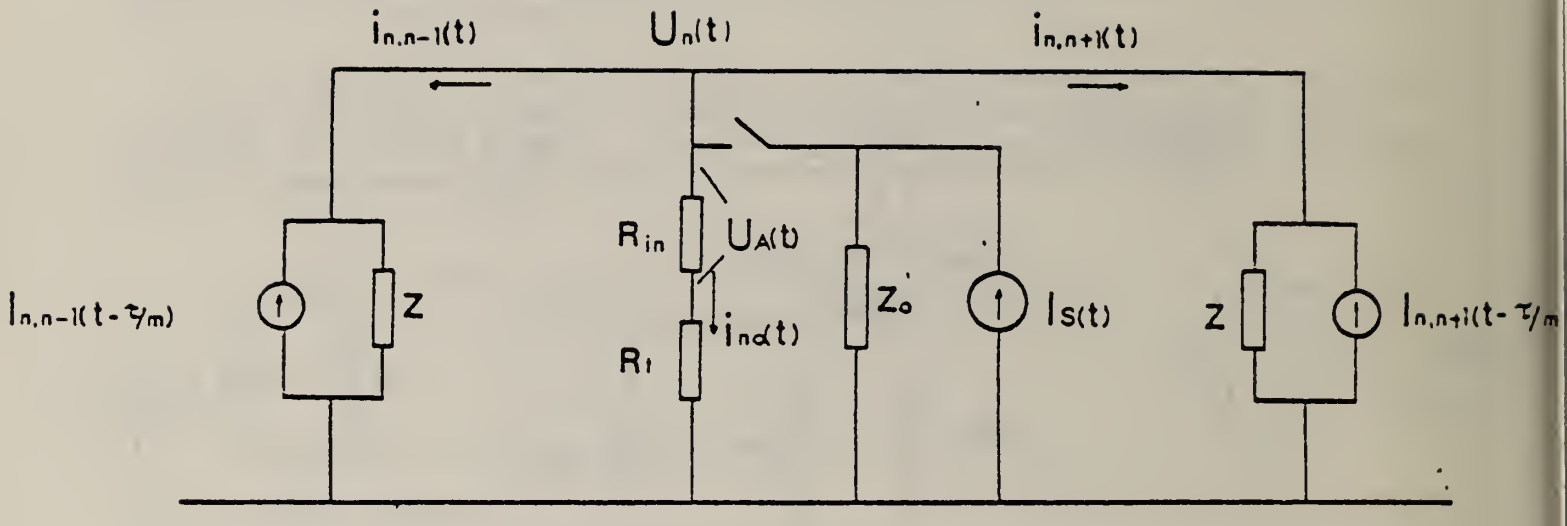

Figure 8. Equivalent circuit model for lightning striking on conductor.

The lightning current source is mathematically simulated as

$$I_s(t) = I_m(e^{-\alpha t} - e^{-\alpha t}) \ , \qquad (9)$$

where $\alpha_1 = 0.0175 \times 10^{-6}$ and $\alpha_2 = 2.2 \times 10^{-6}$.

To maximize the influence of operating voltage, it is assumed that the polarity of operating voltage is opposite to the lightning current, and at its maximum. The results of the study presented here are based on lightning striking on a tower located at the middle of the line, even though the computer program is capable of selecting any striking point.

Figure 9 shows the relationship between lightning current I_s and maximum current passing through active insulators with different tower resistances. Results demonstrate that the maximum current passing through active insulators is approximately proportional to the lightning current and to the tower resistance. For active insulators, which have a limited maximum current capability, the maximum lightning current as a function of tower resistance is shown in figure 10. Within these limits, the active insulators will be able to maintain adequate operation of the transmission system.

The major functions of active insulators are to protect substation equipment under overvoltage conditions and to reduce the duties of station arresters. The maximum overvoltage at substation terminal is shown in figure 11, for tower resistances of up to 30 Ω, while the overvoltage is maintained below 350 kV (1.75 p.u.). The maximum current passing through the station arrester is less than 1.2 kA for lightning currents of up to 200 kA and tower resistance of 30 Ω (fig. 12).

These results indicate that with only four active insulator strings between the location of the lightning strike location and the substation, active insulators can provide substantial protection to the station equipment. Since the voltage across the insulator string is maintained below 600 kV (3.0 p.u.), the back flashover risk is greatly reduced.

The material research facility has been producing much better quality samples in the last two months. Materials with dielectric constants of less than 3.0, volume resistivity of higher than 10^{14}Ω-cm and breakdown voltage of higher than 17 kV/mm have been fabricated and tested. The material composition and processing procedures will be finalized. The study on single-phase transient performance of active insulators will continue in the next quarter. A three-phase mathematical model is currently under development and will be completed. The nonlinear element necessary for producing prototype active insulators will be procured. The design of prototype active insulator unit will be conducted according to the available nonlinear element shape.

For further information, contact Dr. T. C. Cheng (213) 743-6938.

6. INVESTIGATION OF INSULATOR SURFACE FLASHOVER IN GAS
Subtask No. A057

The weakest component of a gas-insulated system is typically the gas solid interface. The basic mechanisms leading to the interfacial breakdown (flashover)

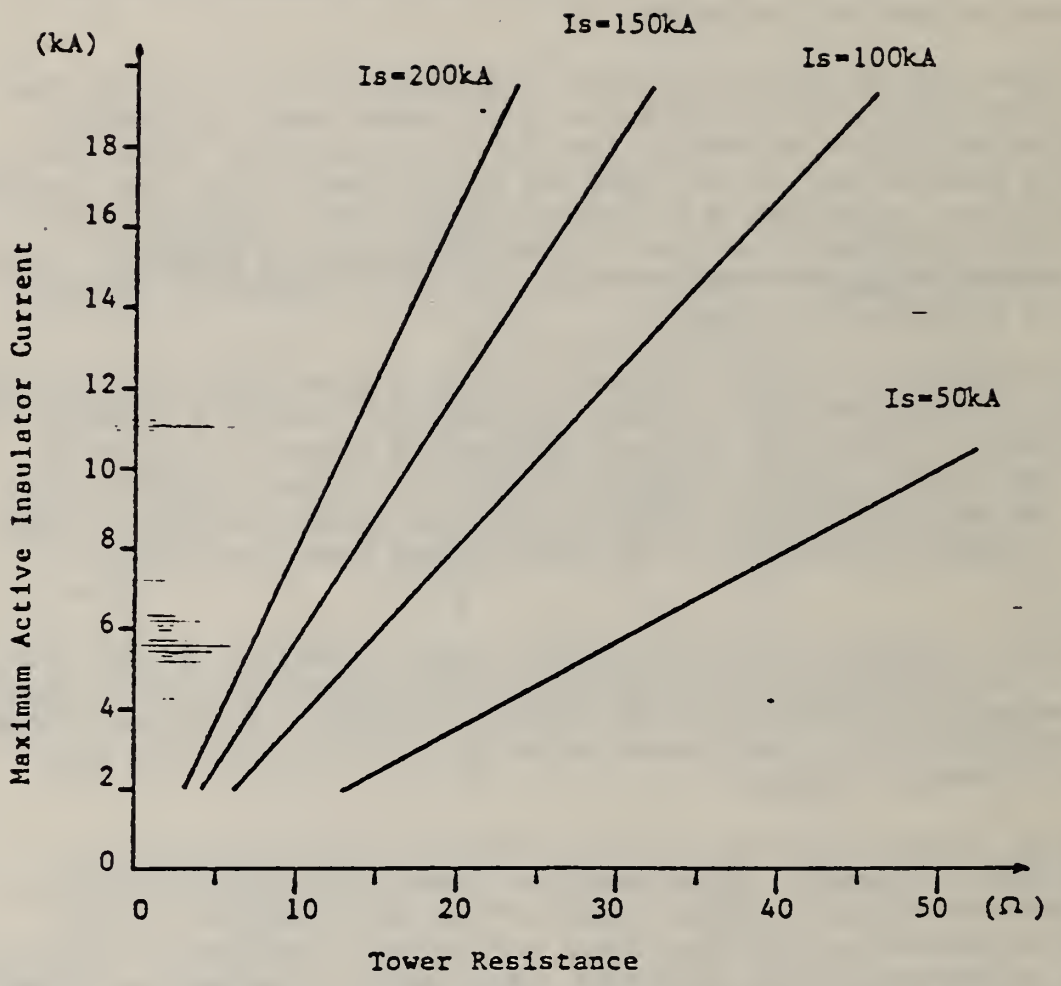

Figure 9. The effect of tower resistance and lightning current on maximum active insulator current.

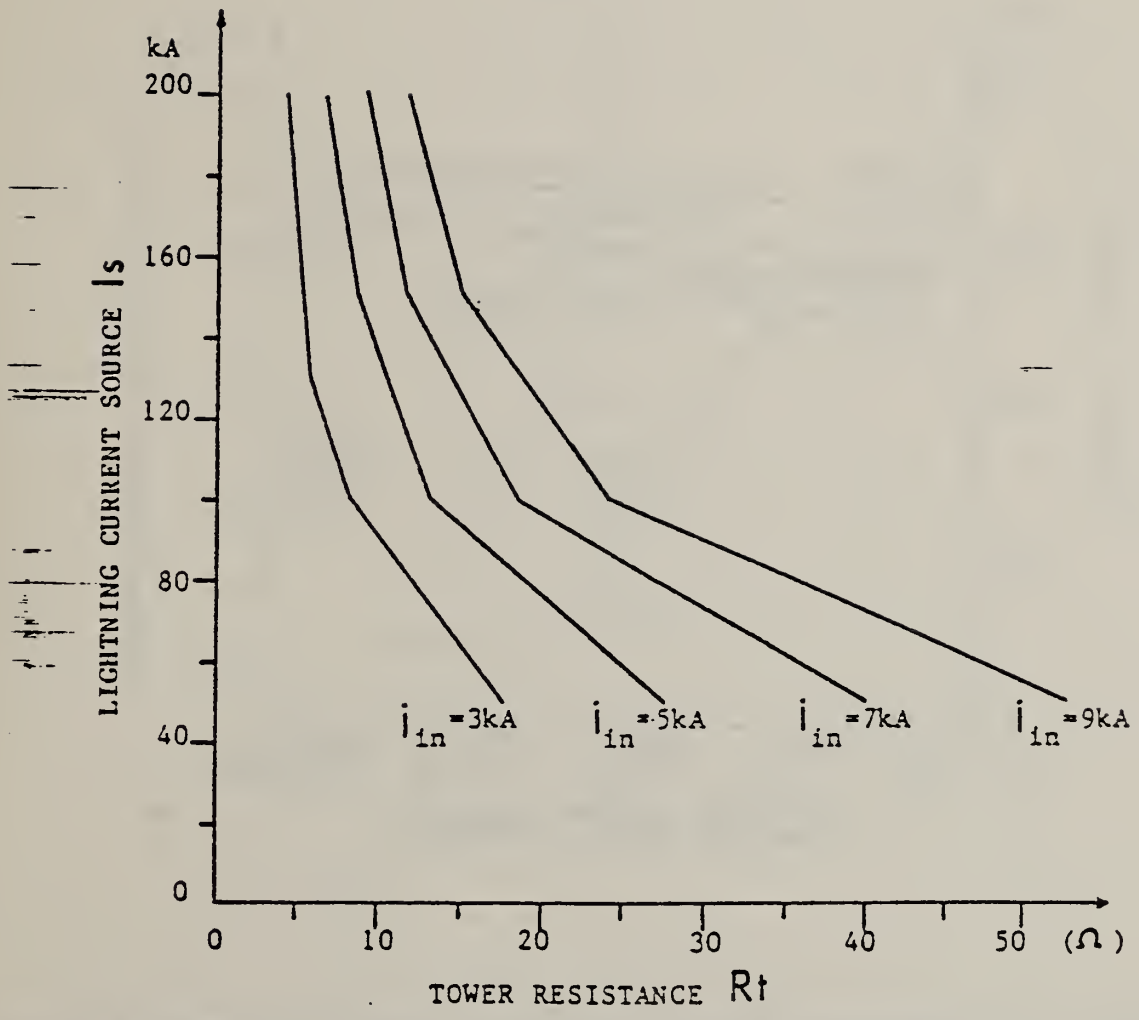

Figure 10. The effect of tower resistance on acceptable lightning current for limited active insulator capacity.

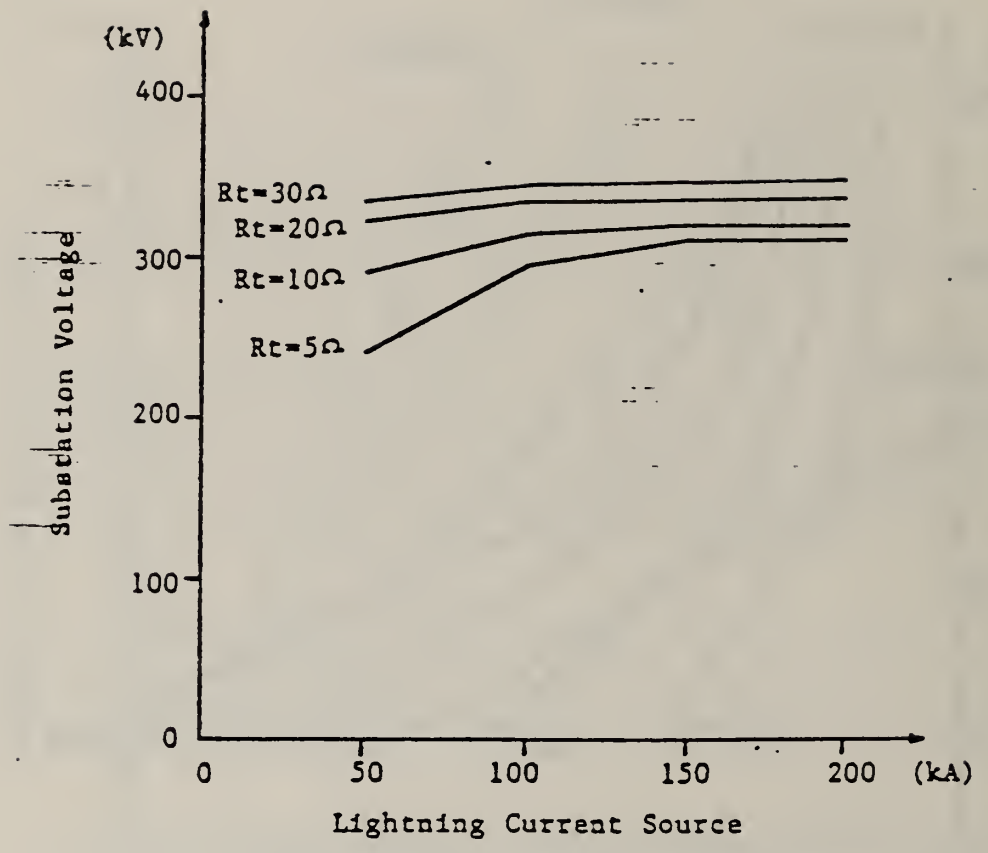

Figure 11. Substation voltage level under a simulated lightning at the middle of the transmission.

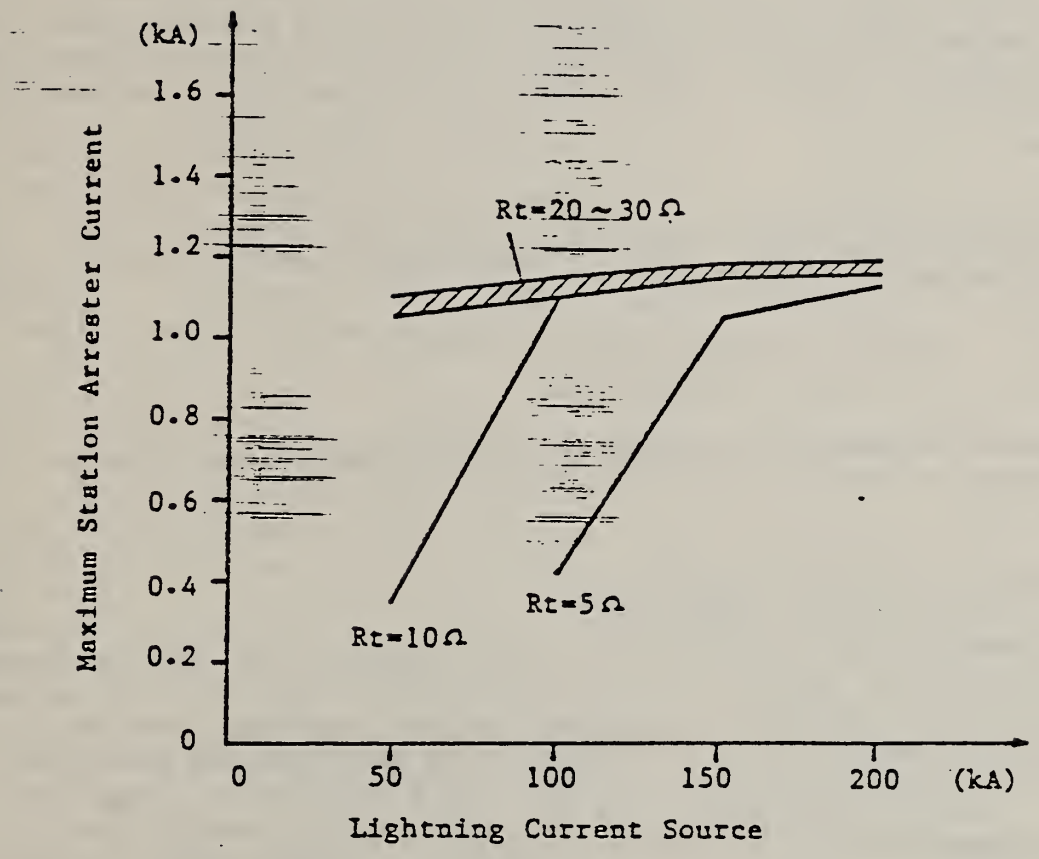

Figure 12. Maximum station arrestor current under a simulated lightning strike at the middle of the transmission line.

and the role of design parameters in the breakdown process are not well enough understood to predict the ultimate system performance levels and/or to affect optimum material and geometry design selections. Research is therefore being conducted to investigate the primary mechanisms associated with insulator surface flashover in practical insulating gas. An additional objective is to determine the role of various geometric and material parameters on the basic flashover mechanisms and the ultimate insulator system performance.

It has been observed that the electrical strength of an electrode arrangement, bridged with a solid/gas interface, is less than that of the same electrodes separated only by insulating gas. It can be postulated that the reduction of insulation strength is associated with primary emission and electron multiplication processes which occur near and along the surface of the bridging insulator. Specific tasks, consistent with the above objectives, have therefore been initiated to investigate surface currents and electric fields associated with a gas/solid interface. Specific tasks, conducted using 60 Hz ac, include:

(1) Measurement of insulator surface currents associated with pre-flashover events,

(2) Electro-optical measurement of interfacial fields associated with pre-breakdown and flashover, and

(3) Development of analog and computer-based numerical techniques for the calculation of insulator surface fields.

This work is being performed by the Department of Electrical and Computer Engineering, University of South Carolina, under a grant from the National Bureau of Standards.

Solid/Gas Interfacial Current Measurements

Insulator surface currents occurring before flashover have been measured. It can be postulated that these currents are associated with insulator surface charging and/or partial discharges along the insulator surface. Insulator surface charging has been previously observed in vacuum insulated systems and results in local enhancement of cathode fields and a reduction of insulation strength [5-7]. Partial discharges along the insulator can result from surface charge enhanced fields (on the insulator) or primary events initiated near the electrodes.

Surface currents have been determined by measuring voltage across a resistor placed in series with gas-insulated electrodes. The experimental arrangement consists of two electrodes placed in a high pressure vessel and a current viewing resistor (CVR). Various electrode geometries, with and without a bridging solid insulator, can be used (including point-plane, rod-plane, and plane-plane) with electrode separations, up to a few centimeters. The pressure vessel permits the use of SF_6, N_2, or other gases and has a maximum operating pressure of approximately 1.38 MPa. The voltage across the CVR is determined using a bridge network which effectively eliminates ac displacement current signals. Excitation voltage is obtained utilizing a 100 kV, 60 Hz, ac transformer, which is partial discharge free up to 40 kV.

Interfacial currents have been measured using the described system for unbridged point-plane and plane-plane and bridged plane-plane geometries in vacuum and nitrogen. Vacuum and unbridged gap data have been obtained to provide a basis of comparison for the bridged gap performance in gas.

Bridged Vacuum Gap

Typical results observed for a 1.27 cm vacuum gap, bridged with a polymethylmethacrylate (PMMA) insulator, are shown in figure 13, which shows the gap excitation voltage and the surface current as observed using the CVR. The general behavior observed is listed below:

(1) Small current "spikes," shown in figure 13(a), occur just before the voltage peaks for relatively low voltages. It should be noted the short current pulse shapes are not necessarily indicative of the actual current pulse temporal performance but are determined by the electrical (impulsed) response of the measurement system.

(2) As the voltage increases the observed fast current pulses occur earlier during the excitation. Additionally, a slower current component begins to form. The fast pulses are observed to occur in addition to this slower component. The slower current component peak occurs prior to the excitation voltage maximum. This performance is shown in figure 13(b).

(3) As the voltage is further increased, the slower current component dominates. As the voltage is further increased, a second, slow current component forms which is in phase with the excitation. This performance is shown in figure 13(c).

(4) At even higher voltage values, the slow current component, which is approximately in phase with the excitation, dominates. This performance is shown in figure 13(d). It should be noted that the current behavior shown is not symmetrical but is polarity dependent, apparently due to unintentional electrode or insulator differences.

It is postulated that the current performance indicated by the data of figure 14 is due to the following mechanisms:

(1) At relatively low voltages, the surface currents are due to short duration partial discharges near the cathode.

(2) At higher voltage levels, more substantial currents are observed due to increased cathode electron emission near the insulator/cathode junction. The emitted electrons strike the insulator and cause positive charging of the insulator due to the greater than unity secondary emission coefficient of PMMA. The charging currents continue to flow until the insulator reaches a steady-state charge value and accepts no more charge. The peak of the surface charging current, therefore, does not occur at the same time as the voltage peak.

(3) At higher voltage levels, field emission currents, which do not flow along the insulator, begin to dominate. Field emission current corresponds to the current which is approximately in phase with the excitation. It has been previously observed that these in phase currents obey Fowler-Nordheim predictions [8]. This implies that the electron interactions with the insulator surface are minimal for these currents.

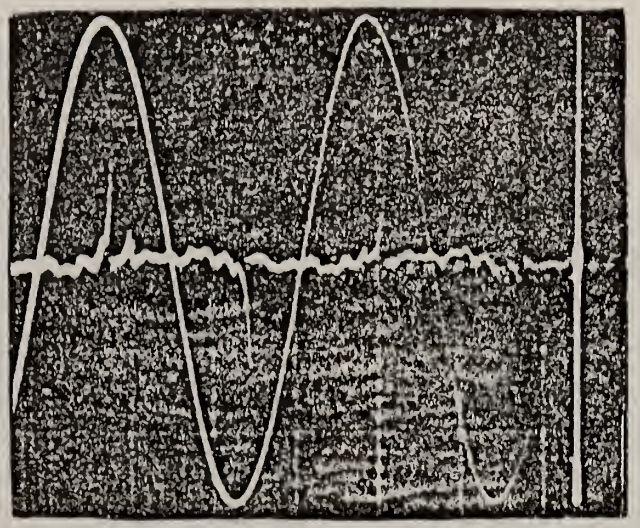

(a) 3.86 kV/div, 1.5 μA/div, 5ms/div

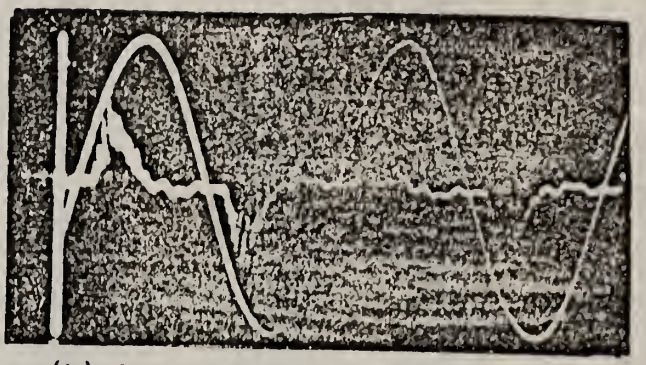

(b) 22 kV/div, 9 μA/div, 5ms/cm

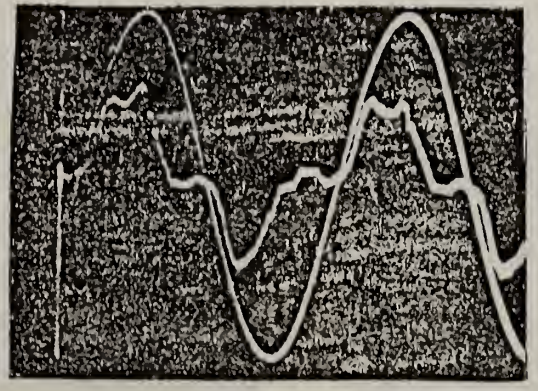

(c) 36 kV/div, 36 μA/div, 5ms/div

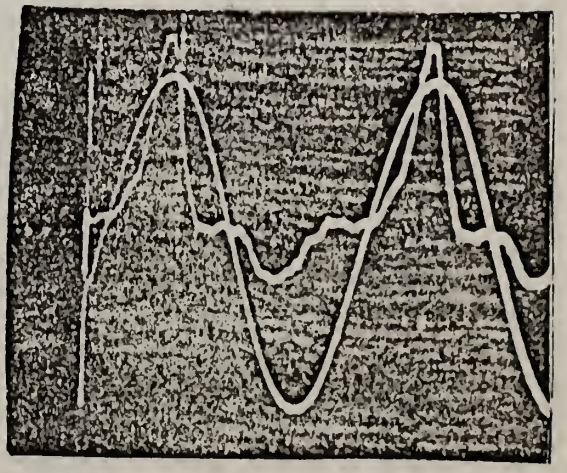

(d) 8.5 kV/div, 4.5 μA/cm, 5ms/cm

Figure 13. Pre-flashover currents, vacuum, 1.27 cm PMMA insulator. 60 Hz signal is voltage, other is current.

(4) It can be further postulated that flashover occurs in vacuum due to electron avalanches, near the insulator surface, in gas which has been desorbed from the insulator by the incident and cascading electrons.

Unbridged Gas-Filled Gap

Pre-flashover, current measurements have also been conducted using a point-plane geometry (2.8 cm separation) in nitrogen. Typical results are shown in figure A which shows the excitation voltage and the CVR response. These data indicate that partial discharges (pd) occur near the peak of the excitation. Sufficient data have been obtained to determine that the pd inception and extinction voltages are linear functions of the gas pressure. It has been found that pd inception and extinction occur at 16 kV and 14.8 kV, respectively, at a pressure of 448 kPa. The data, in addition to indicating the behavior of an unbridged gap for comparison purposes, do indicate satisfactory operation of the diagnostic system.

Bridged Gap in Nitrogen

Pre-flashover current measurements have also been obtained for a bridged gap in nitrogen. The electrode arrangement consisted of a 5 cm diameter lower electrode and a 7.28 cm diameter upper electrode. A 1.27 cm diameter, 0.635 cm high, cylindrical PMMA insulator was placed between the electrodes. The electrodes, in this arrangement, were separated by the insulator and a nitrogen gap of length d, between the insulator top and the upper electrode. The pd inception voltage was measured, using the CVR, for d values from 0 to 0.5 cm.

Typical current pulses are shown in figure 15 for d = 0.2 cm. The current pulses are positive. The negative undershoot is due to the detection circuit response. The observed pulses are short and are, again, indicative of the measurement circuit impulse response. Only the response amplitude and time of occurrence are considered as significant data. The upper electrode is the anode for the data shown. Similar current pulses are observed, but with a greater repetition rate, when the upper electrode is the cathode. The pulse repetition rate decreases substantially when d is decreased to zero.

The data of figures 15, 16, and 17 and considerable additional data of this same type imply that, for an electrode arrangement with an insulator present;

(1) The pd rate is considerably lower than the pd rate observed for point-plane, unbridged gap (fig. 14).

(2) The pd rate decreases to a small value when d goes to zero, corresponding to electrodes with an insulator bridging the entire gap.

(3) The difference between the inception and breakdown voltage is less for d = 0 than for non-zero values of d.

(4) The inception, extinction, and breakdown voltage are linear functions of p for all values of d.

Figure 14. Pre-flashover currents, point-plane (2.86 cm), nitrogen, 5 psig, 3.48 kV/div, 1 ms/div.

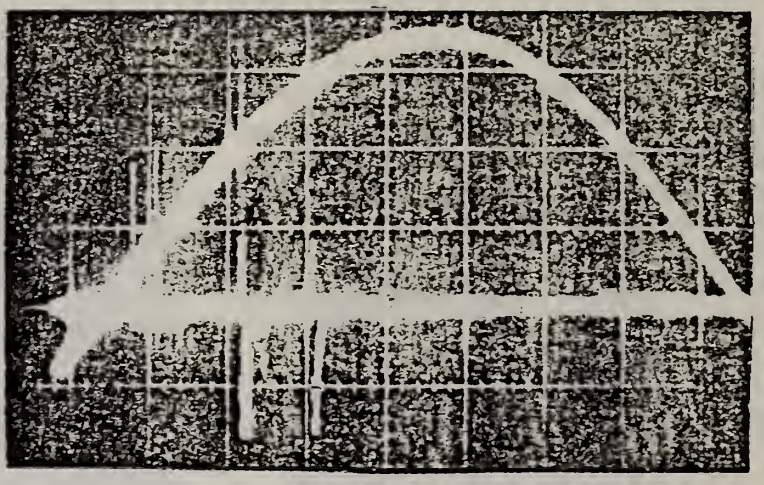

Figure 15. Pre-flashover currents, bridged gap, nitrogen, 5 psig, d = 0.2 cm, 3.78 kV/div, 1 ms/div.

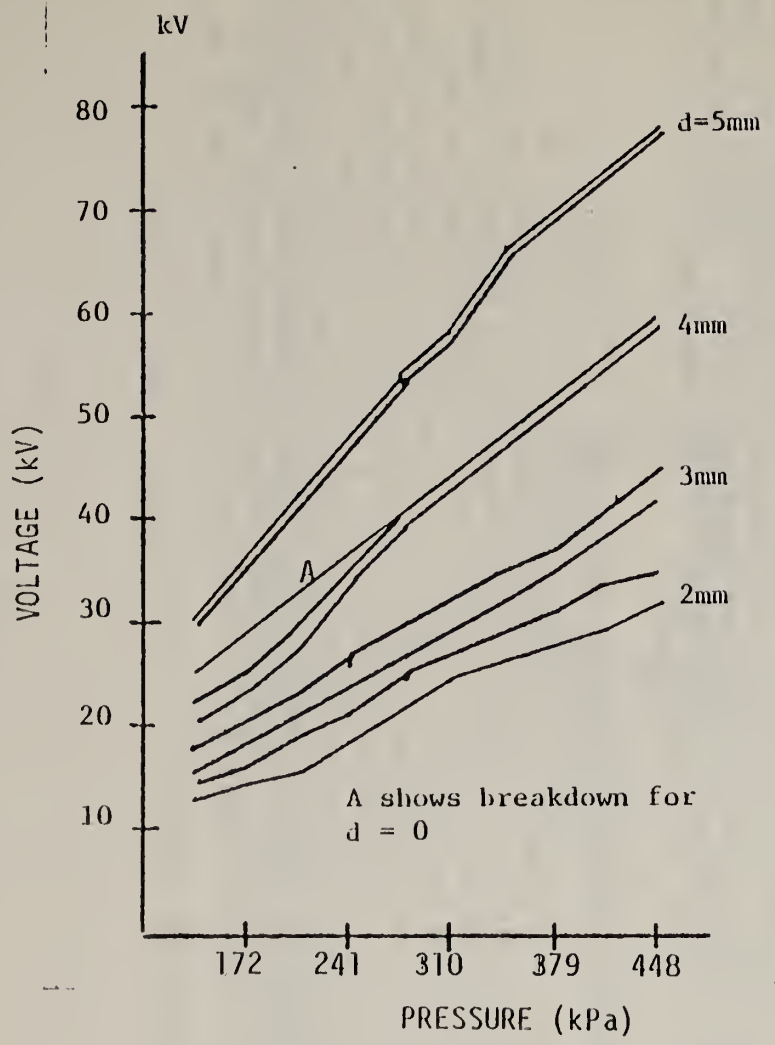

Figure 16. Pd inception (upper) and extinction voltage, d is nitrogen gap size, PMMA insulation 0.635 cm in nitrogen.

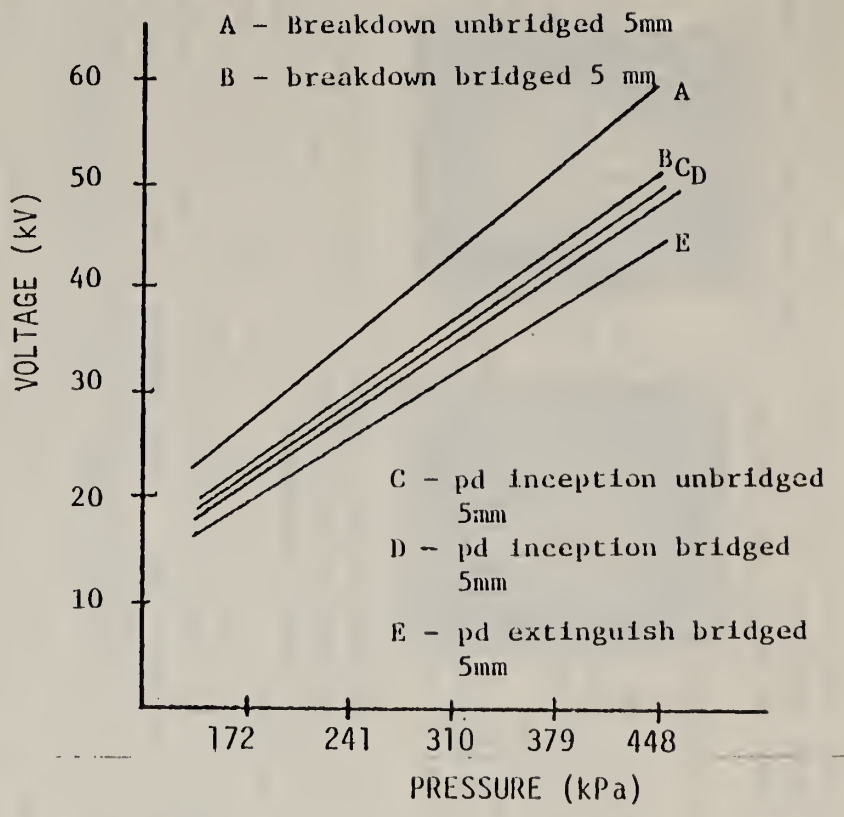

Figure 17. Inception, breakdown, and extinction voltages, bridged and unbridged gap in nitrogen.

(5) The data imply that surface currents do flow. The relationship between the amplitude and repetition rate of the currents and observed inception and breakdown voltages are presently being determined.

Electro-Optical Surface Field Measurements

Insulator surface charging can be postulated to be a mechanism associated with the flashover process. The current measurements reported above can be interpreted as currents flowing along the insulator surface which can contribute to surface charging. An electro-optical surface field measurement technique has previously been reported which directly measures the interfacial electric fields at the gas/solid interface [5,6,7,9]. Results obtained using this technique have also previously been reported, primarily for vacuum/solid interfaces.

Measurements have most recently been obtained for a gas/solid interface. However, for long pulsed or 60 Hz ac excitations a problem has been encountered using the nitrobenzene sensing liquid. Typical results obtained using an unbridged gap are shown in figure 18. This figure shows an interference pattern using a 1 ms risetime, long pulse excitation. This figure and similar additional data show a density perturbation which occurs in the nitrobenzene for times longer than approximately 1 ms. This density perturbation obscures the interference pattern being used to determine the interfacial fields and is probably due to charge injection, from the electrodes, into the nitrobenzene [3,4].

The observed perturbation is undesirable. Attempts have been made to eliminate the perturbation by removing water from the nitrobenzene using a molecular seive and a recirculation pump system. Nitrobenzene resistivities on the order of 10 Ω-cm have been produced. However, the perturbation problem continued to exist.

More recently, the test cell arrangement used has been modified such that no charge injection from the electrodes can occur. The test arrangement is shown in figure 19 and consists of a glass tube of rectangular cross section which contains the nitrobenzene without liquid contact with the electrodes. Tests are currently being conducted to determine if charge injection and resulting liquid density perturbations occur with this arrangement.

Electric Field Predictor and Calculation Techniques

Both analog and digital electric field calculation techniques are being developed. It is important to develop these techniques to support the experimental measurements of the surface electric fields. An electrolytic tank has been constructed and is now operational. With this arrangement, the electric fields associated with various electrode-insulator configurations can be determined and compared with those electro-optically measured. A computer solution to Laplace's equation, appropriate to the experimental configurations being used, has also been developed. With this digital technique, the fields associated with various electrode and insulator geometries and various surface charge distributions can now be predicted and the results compared with the electro-optical results to be obtained.

For further information, contact Dr. J. E. Thompson, (803) 777-7304.

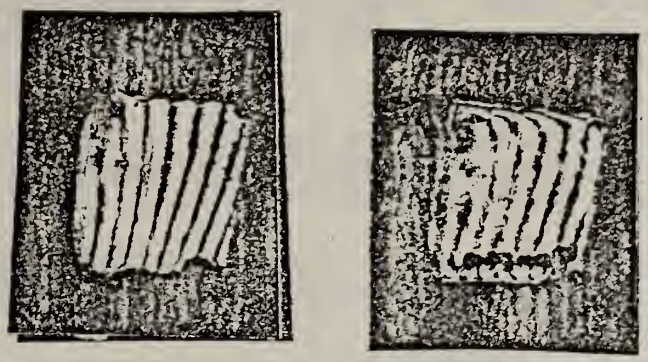

no field

with field showing
density perturbation
at cathode (1.1 ms)

Figure 18. Interference pattern indicative of electric field distribution, no interface.

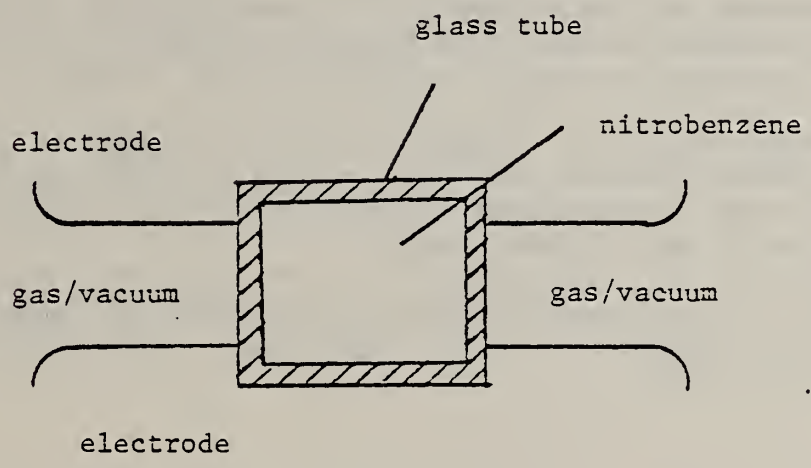

Figure 19. Electro-optical field measurement insulator arrangement.

7. REFERENCES

[1] R. J. Van Brunt and D. A. Leep, "Corona-Induced Decomposition of SF_6," Proc. 3rd Int'l Symp. on Gaseous Dielectrics, Gaseous Dielectrics III, pp. 402-409, 1982.

[2] R. J. Van Brunt, "Effects of H_2O on the Behavior of SF_6 Corona," Proc. 7th Int. Conf. on Gas Discharges and Their Applications, London, pp. 255-258, 1982.

[3] R. E. Hebner, R. A. Malewski, and E. C. Cassidy, "Optical Methods of Electrical Measurement at High Voltage Levels," Proc. IEEE, Vol 65, pp. 1524-1548, 1977.

[4] E. J. Hopfinger and J. P. Gosse, "Charge Transport by Self-Generated Turbulence in Insulating Liquids Submitted to Unipolar Injection," Phys. Fluids, Vol. 14, pp. 1671-1682, 1971.

[5] J. E. Thompson, J. Lin, K. Mikkelson, and M. Kristiansen, "Optical Measurements of Insulator Surface Charging," Appl. Phys. Lett., Vol 37, pp. 574-376, 1980.

[6] J. E. Thompson, J. Lin, K. Mikkelson, and M. Kristiansen, "Investigations of Fast Insulator Surface Flashover," IEEE Trans. Plasma Science, Vol PS-8, pp. 191-197, 1980.

[7] R. Lee, H. Rhinehart, J. E. Thompson, and T. S. Sudarshan, "Predischarge Current Measurements and Optical Surface Field Measurements Associated with Insulator Surface Flashover," in Gaseous Electronics III, edited by Loucas G. Christophorou, Pergamon Press, pp. 349-355, 1982.

[8] R. Lee, T. S. Sudarshan, J. E. Thompson, and R. L. Boxman, "Predischarge Current Measurements in Vacuum Gaps Bridged with Plexiglas Insulators," Proc. 10th Int. Symp. on Discharges and Electrical Insulation in Vacuum, Columbia, SC, pp. 288-296, 1982.

[9] J. E. Thompson, M. Kristiansen, and M. O. Hagler, "Optical Measurements of High Electric and Magnetic Fields," IEEE Trans. Instrum. and Meas., Vol IM-25, pp. 1-7, 1976.

NBS-114A (REV. 2-8C)

U.S. DEPT. OF COMM. BIBLIOGRAPHIC DATA SHEET (See instructions)	1. PUBLICATION OR REPORT NO. NBSIR 83-2755	2. Performing Organ. Report No.	3. Publication Date September 1983

4. TITLE AND SUBTITLE

Development of Power System Measurements -- Quarterly Report
October 1, 1982 to December 31, 1982

5. AUTHOR(S)

R. E. Hebner, Editor

6. PERFORMING ORGANIZATION (If joint or other than NBS, see instructions)

NATIONAL BUREAU OF STANDARDS
DEPARTMENT OF COMMERCE
WASHINGTON, D.C. 20234

7. Contract/Grant No.

8. Type of Report & Period Covered

9. SPONSORING ORGANIZATION NAME AND COMPLETE ADDRESS (Street, City, State, ZIP)

Prepared for
Department of Energy
Division of Electric Energy Systems
1000 Independence Avenue, SW
Washington, DC 20585

10. SUPPLEMENTARY NOTES

☐ Document describes a computer program; SF-185, FIPS Software Summary, is attached.

11. ABSTRACT (A 200-word or less factual summary of most significant information. If document includes a significant bibliography or literature survey, mention it here)

This report documents the progress on five technical investigations sponsored by the Department of Energy and performed by the Electrosystems Division, the National Bureau of Standards. The work described covers the period from October 1, 1982 to December 31, 1982. The report emphasizes the calibration of instruments designed to measure the 60-Hz electric and magnetic fields in biological exposure facilities, the measurement of the rate of decomposition of SF_6 in positive dc-corona discharges, and in the measurement of space charge in transformer oil between 100°C and 150°C.

12. KEY WORDS (Six to twelve entries; alphabetical order; capitalize only proper names; and separate key words by semicolons)

cables; composite insulation; dc fields; high voltage; incipient fault; insulation; liquid breakdown; SF_6; space charge; transformer oil.

13. AVAILABILITY

☒ Unlimited
☐ For Official Distribution. Do Not Release to NTIS
☐ Order From Superintendent of Documents, U.S. Government Printing Office, Washington, D.C. 20402.
☒ Order From National Technical Information Service (NTIS), Springfield, VA. 22161

14. NO. OF PRINTED PAGES 40

15. Price $8.50

USCOMM-DC 6043-P80